LETTERS

NLRP3 inflammasomes are required for atherogenesis and activated by cholesterol crystals

Peter Duewell[1,3]*, Hajime Kono[2]*, Katey J. Rayner[4,5], Cherilyn M. Sirois[1], Gregory Vladimer[1], Franz G. Bauernfeind[6], George S. Abela[8], Luigi Franchi[9], Gabriel Nuñez[9], Max Schnurr[3], Terje Espevik[10], Egil Lien[1], Katherine A. Fitzgerald[1], Kenneth L. Rock[2], Kathryn J. Moore[4,5], Samuel D. Wright[11], Veit Hornung[5]* & Eicke Latz[1,7,10]*

The inflammatory nature of atherosclerosis is well established but the agent(s) that incite inflammation in the artery wall remain largely unknown. Germ-free animals are susceptible to atherosclerosis, suggesting that endogenous substances initiate the inflammation[1]. Mature atherosclerotic lesions contain macroscopic deposits of cholesterol crystals in the necrotic core, but their appearance late in atherogenesis had been thought to disqualify them as primary inflammatory stimuli. However, using a new microscopic technique, we revealed that minute cholesterol crystals are present in early diet-induced atherosclerotic lesions and that their appearance in mice coincides with the first appearance of inflammatory cells. Other crystalline substances can induce inflammation by stimulating the caspase-1-activating NLRP3 (NALP3 or cryopyrin) inflammasome[2,3], which results in cleavage and secretion of interleukin (IL)-1 family cytokines. Here we show that cholesterol crystals activate the NLRP3 inflammasome in phagocytes *in vitro* in a process that involves phagolysosomal damage. Similarly, when injected intraperitoneally, cholesterol crystals induce acute inflammation, which is impaired in mice deficient in components of the NLRP3 inflammasome, cathepsin B, cathepsin L or IL-1 molecules. Moreover, when mice deficient in low-density lipoprotein receptor (LDLR) were bone-marrow transplanted with NLRP3-deficient, ASC (also known as PYCARD)-deficient or IL-1α/β-deficient bone marrow and fed on a high-cholesterol diet, they had markedly decreased early atherosclerosis and inflammasome-dependent IL-18 levels. Minimally modified LDL can lead to cholesterol crystallization concomitant with NLRP3 inflammasome priming and activation in macrophages. Although there is the possibility that oxidized LDL activates the NLRP3 inflammasome *in vivo*, our results demonstrate that crystalline cholesterol acts as an endogenous danger signal and its deposition in arteries or elsewhere is an early cause rather than a late consequence of inflammation. These findings provide new insights into the pathogenesis of atherosclerosis and indicate new potential molecular targets for the therapy of this disease.

Cholesterol, an indispensable lipid in vertebrates, is effectively insoluble in aqueous environments, and elaborate molecular mechanisms have evolved that regulate cholesterol synthesis and its transport in fluids[4]. Cholesterol crystals are recognized as a hallmark of atherosclerotic lesions[5] and their appearance assists the histopathological classification of advanced atherosclerotic lesions[6]. However, crystalline cholesterol is soluble in the organic solvents used in histology, so that the presence of large crystals is identifiable but only indirectly as so-called cholesterol crystal clefts, which delineate the space that was occupied before sample preparation[7]. The large cholesterol crystal clefts in atherosclerotic plaques were typically observed only in advanced lesions; crystal deposition was therefore thought to arise late in this disease. However, given that atherosclerosis is intimately linked to cholesterol levels, we were interested to determine when and where cholesterol crystals first appear during atherogenesis.

We fed atherosclerosis-prone Apo-E-deficient mice on a high cholesterol diet to induce atherosclerosis[8,9] and used a combination of laser reflection and fluorescence confocal microscopy[3] to identify crystalline materials and immune cells. Many small crystals appeared as early as two weeks after the start of the atherogenic diet within small accumulations of subendothelial immune cells in very early atherosclerotic sinus lesions (Fig. 1a, b and Supplementary Figs 1 and 2). The reflective material was identified by filipin staining as being mostly cholesterol crystals (not shown). Crystal deposition and immune-cell recruitment increased steadily with diet feeding, and the appearance of crystals was correlated with that of macrophages ($r^2 = 0.99$, $P < 0.001$) (Fig. 1a–e). Cholesterol crystals were detected not only in necrotic cores but also in subendothelial areas and found to localize both inside and outside cells (Fig. 1b). In corresponding haematoxylin/eosin-stained sections cholesterol crystal clefts were visible only after 8 weeks of diet, and smaller crystals remained invisible (Fig. 1a). As expected, we failed to detect macrophages or accumulation of crystals in the aortic sinus sections in mice fed on a regular chow diet (Fig. 1a, b, bottom panels). In addition, in human atherosclerotic lesions small crystals were abundant in areas rich in immune cells (Supplementary Figs 3 and 4). These studies establish that crystals emerge at the earliest time points of diet-induced atherogenesis together with the appearance of immune cells in the subendothelial space.

Various crystals that are linked to tissue inflammation, as well as pore-forming toxins or extracellular ATP, can activate IL-1 family cytokines through the triggering of NLRP3 (ref. 10). Of note, cellular priming through nuclear factor (NF)-κB activation leads to the induction of pro-forms of the IL-1 family cytokines and NLRP3 itself, a step that is required for NLRP3 activation, at least *in vitro*[11]. To test whether cholesterol crystals could activate the release of IL-1β, we incubated lipopolysaccharide (LPS)-primed human peripheral blood mononuclear cells (PBMCs) with cholesterol crystals. Cholesterol crystals induced a robust, dose-responsive release of cleaved IL-1β

[1]Department of Infectious Diseases and Immunology and [2]Department of Pathology, University of Massachusetts Medical School, Worcester, Massachusetts 01605, USA. [3]Department of Medicine, Division of Gastroenterology, University of Munich, 80336 Munich, Germany. [4]Leon H. Charney Division of Cardiology, New York University, New York, New York 10016, USA. [5]Harvard Medical School, Lipid Metabolism Unit, Massachusetts General Hospital, Boston, Massachusetts 02114, USA. [6]Institute of Clinical Chemistry and Pharmacology and [7]Institute of Innate Immunology, University Hospitals, University of Bonn, 53127 Bonn, Germany. [8]Department of Medicine, Division of Cardiology, Michigan State University, East Lansing, Michigan 48824, USA. [9]Department of Pathology, University of Michigan Medical School, Ann Arbor, Michigan 48109, USA. [10]Institute of Cancer Research and Molecular Medicine, Norwegian University of Science and Technology, Trondheim, 7491, Norway. [11]Cardiovascular Therapeutics, CSL Limited, Parkville, Victoria 3052, Australia. *These authors contributed equally to this work.

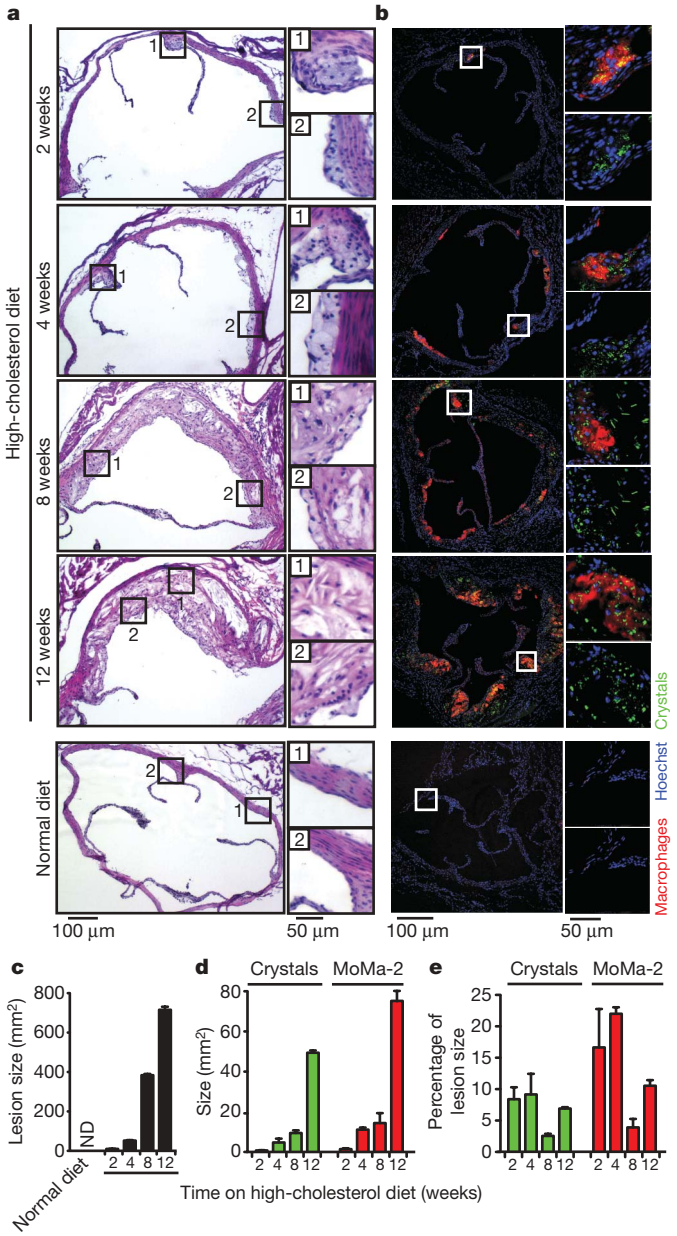

Figure 1 | Cholesterol crystals appear in early atherosclerotic lesions. **a**, **b**, Haematoxylin/eosin staining (**a**) and confocal fluorescence and reflection microscopy (**b**) of adjacent aortic sinus sections of Apo-E knockout mice fed on a high-cholesterol diet as indicated or on a normal diet (bottom panels). Areas in white or black boxes are shown enlarged; the crystal reflection signal is colour-coded green. **c**–**e**, Quantification of lesion size (**c**), amount of crystal or macrophage marker MoMa-2 staining presented as absolute values (**d**) or as a percentage of lesion size (**e**). ND, not detected. In **a** and **b** sections representative of three mice from each group are shown. Means and s.e.m. are shown in **c**, **d** and **e**.

in a caspase-1-dependent manner (Fig. 2a, b). Cholesterol crystals added to unprimed cells did not release IL-1β into the supernatant, indicating the absence of any contaminants that would be sufficient for the priming of cells (Fig. 2a)[11]. IL-1 cytokines are processed by caspase-1, which can be activated by various inflammasomes[9]. Indeed, as previously observed with other crystals, cholesterol crystals induced caspase-1 cleavage and IL-1β release in wild-type but not in NLRP3-deficient or ASC-deficient macrophages (Fig. 2c, d). Transfected double-stranded DNA (poly(dA-dT)•poly(dT-dA)), a control activator that induces the AIM-2 inflammasome[12], activated caspase-1 and induced IL-1β release in an ASC-dependent but NLRP3-independent manner, as expected (Fig. 2c, d). In addition, mouse macrophages also produced cleaved IL-18, another IL-1 family member that is processed by inflammasomes (Supplementary Fig. 5a). We also found that chemically pure synthetic cholesterol crystals activated NLRP3, providing further evidence that cholesterol crystals themselves rather than contaminating molecules were the biologically active material (Supplementary Fig. 5b). Priming of cells for NLRP3 activation could be achieved by other pro-inflammatory substances such as cell wall components of Gram-positive bacteria (Supplementary Fig. 5c). Moreover, minimally modified low-density lipoprotein (LDL) also primed cells for NLRP3 activation (Supplementary Fig. 5d)[13]. Taken together, these data establish that crystalline cholesterol leads to NLRP3 inflammasome activation in human and mouse immune cells.

For further elucidation of the mechanisms involved in cholesterol crystal recognition, we inhibited phagocytosis pharmacologically with cytochalasin D or lantriculin A. We found that these agents inhibited NLRP3 activation by crystals but not by the AIM2 activator poly(dA-dT)•poly(dT-dA) (Fig. 3a and Supplementary Fig. 6a, c, d). To follow the fate of the internalized particles, we analysed macrophages incubated with cholesterol crystals by combined confocal reflection and fluorescence microscopy. Cholesterol crystals induced profound swelling in a fraction of cells (Fig. 3b), as observed for other aggregated materials[3,14]. Phagolysosomal membranes contain lipid raft components[15], which allowed us to stain the surface of cells with the raft marker choleratoxin B labelled with one fluorescent colour and also to label internal phagolysosomal membranes after cell permeabilization with differently fluorescing choleratoxin B. Indeed, in macrophages that had previously ingested cholesterol crystals, this staining revealed that some cholesterol crystals lacked phagolysosomal membranes and resided in the cytosol of a fraction of cells, thus indirectly indicating crystal-induced phagolysosomal membrane rupture (Fig. 3c). This finding was further supported by crystal-induced translocation of soluble lysosomal markers into the cytosol (see below). In addition, cholesterol crystals dose-responsively led to a loss of lysosomal acridine orange fluorescence, further confirming lysosomal disruption (Supplementary Fig. 6e). These studies suggest that cholesterol-crystal-induced lysosomal damage in macrophages leads to the translocation of phagolysosomal content into the cytosol. In further experiments we found that the inhibition of lysosomal acidification or cathepsin activity blocked the ability of cholesterol crystals to induce IL-1β secretion (Supplementary Fig. 6f). Similarly, analysis of cells from mice deficient in single cathepsins (B or L) also showed that cholesterol crystals led to a diminished release of IL-1β in comparison with wild-type cells. However, the dependence of cholesterol-crystal-induced IL-1β release on single cathepsins was less pronounced at higher doses, suggesting functional redundancy of cathepsin B and L or potentially additional proteases (Fig. 3d). Taken together, these experiments suggest that cholesterol crystals induce translocation of the lysosomal proteolytic contents, which can be sensed by the NLRP3 inflammasome by as yet undefined mechanisms.

It has previously been demonstrated that oxidized LDL, a major lipid species deposited in vessels, has the potential to damage lysosomal membranes[16]. We found that macrophages incubated with oxidized LDL internalized this material and nucleated crystals in large, swollen, phagolysosomal compartments (Fig. 3e); in some cells these compartments ruptured with translocation of the fluorescent marker dye into the cytosol (Fig. 3e, arrows). A time-course analysis revealed that small crystals appeared as early as 1 h after incubation with oxidized LDL (not shown), and larger crystals were visible after longer incubation times (Fig. 3f). It is likely that cholesterol crystals form as a result of the activity of acid cholesterol ester hydolases, which transform cholesteryl esters supplied by oxidized LDL into free cholesterol. As indicated above, minimally modified LDL can prime cells for the NLRP3 inflammasome activation (Supplementary Fig. 5d). Recent evidence suggests that this priming proceeds through the activation of a TLR4/6 homodimer and CD36 (ref. 13). This, together with the propensity of minimally modified LDL to form

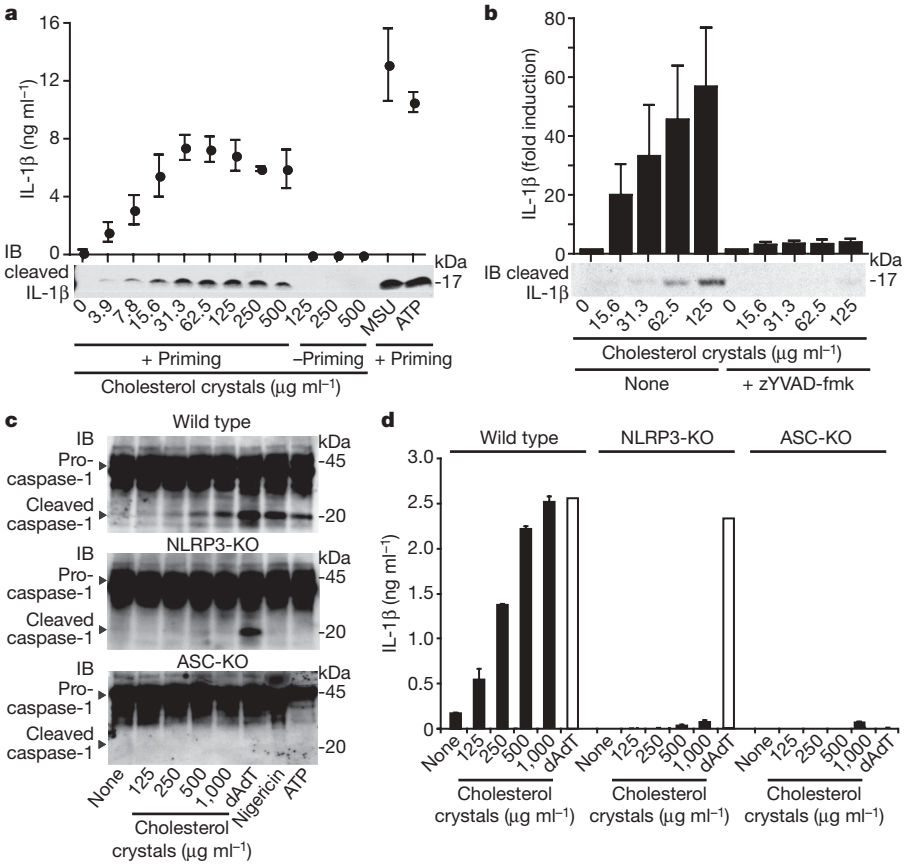

Figure 2 | Cholesterol crystals activate the NLRP3 inflammasome. **a**, **b**, Resting or LPS-primed human PBMCs were treated with cholesterol crystals as indicated, monosodium urate (MSU) crystals (250 μg ml^{-1}) or ATP in the absence (**a**) or presence (**b**) of the caspase-1 inhibitor zYVAD-fmk (10 μM). ELISA and immunoblotting (IB) were performed for IL-1β. **c**, **d**, IB for caspase-1 in supernatants and cell lysates (**c**) or ELISA for IL-1β in supernatants (**d**) from LPS-primed wild-type, NLRP3-deficient (KO) or ASC-deficient macrophages stimulated with cholesterol crystals, transfected double-stranded DNA (poly(dA-dT)•poly(dT-dA)), nigericin or ATP. Means and s.e.m. for four donors are shown in **a** and **b**; one out of three independent experiments is shown in each of **c** and **d**.

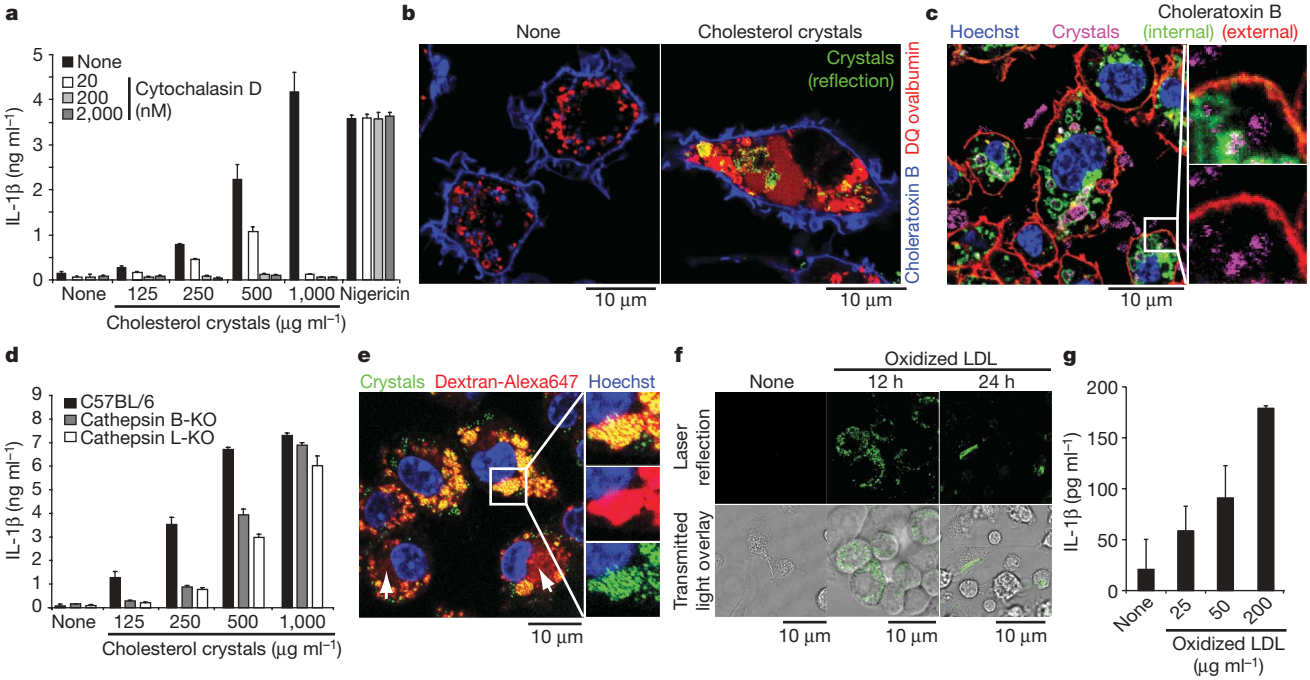

Figure 3 | Cholesterol crystals activate the NLRP3 inflammasome by inducing lysosomal damage. **a**, IL-1β ELISA of supernatants from LPS-primed mouse macrophages stimulated with cholesterol crystals or nigericin in the presence or absence of cytochalasin D. **b**, **c**, Combined confocal fluorescence and reflection microscopy of mouse macrophages incubated with DQ ovalbumin alone (**b**, left) or together with cholesterol crystals (125 μg ml^{-1}) (**b**, right; **c**) for 2 h; plasma membrane was stained with Alexa647-conjugated choleratoxin B (**b**, **c**). **c**, Cells were fixed and permeabilized (0.05% saponin) and internal membranes were additionally stained with Alexa555-conjugated choleratoxin B. Nuclei were stained with Hoechst dye. **d**, IL-1β ELISA of supernatants from LPS-primed mouse macrophages stimulated with cholesterol crystals. **e**, **f**, Mouse macrophages stimulated with oxidized LDL for the indicated durations and fluorescent dextran (**e**, 20 h) were imaged by combined confocal fluorescence and reflection microscopy. **g**, Unprimed mouse macrophages were incubated for 24 h with oxidized LDL as indicated, and IL-1β in supernatants was measured by ELISA. In each of **a**, **d** and **g**, one of three independent experiments is shown (means and s.d.). Representative images of five (**b**, **c**) and two (**e**, **f**) independent experiments are shown.

crystals and to rupture lysosomal membranes, suggests that these LDL species could be sufficient to provide both signals 1 and 2 needed to activate IL-1β release from cells. Indeed, after 24 h of incubation we observed a spontaneous release of IL-1β in the absence of further stimulation of NLRP3 inflammasomes (Fig. 3g).

In mouse atherosclerotic lesions we identified not only macrophages and dendritic cells but also neutrophils accumulated within the intima space (see Supplementary Fig. 2). IL-1β has a key function in the recruitment of neutrophils, and the IL-1-dependent intraperitoneal accumulation of neutrophils has frequently been used as an *in vivo* assay for inflammasome activation and IL-1 production[2,17,18]. Using this acute inflammation model we found that cholesterol crystals induced a robust induction of neutrophil influx into the peritoneum (Fig. 4a). Neutrophil influx into the peritoneum after deposition of cholesterol crystals was markedly decreased in mice lacking IL-1 or the IL-1 receptor (IL-1R), indicating that IL-1 production is indeed induced and essential for cholesterol-crystal-induced inflammation *in vivo*. Moreover, mice lacking NLRP3 inflammasome components or cathepsins B or L also recruited significantly fewer neutrophils into the peritoneum than wild-type mice after injection of cholesterol crystals. However, the decrease in neutrophilic influx observed after deposition of cholesterol crystals was more pronounced in mice lacking IL-1-related genes than in mice lacking NLRP3-inflammasome-related genes (Fig. 4a), presumably because of the contribution of IL-1α signalling and/or caspase-1-independent processing of IL-1β (ref. 19) *in vivo*. In any case, these data confirm that cholesterol crystals trigger NLRP3 inflammasome-dependent IL-1 production *in vivo*.

To test whether the NLRP3 inflammasome is involved in the chronic inflammation that underlies atherogenesis in vessel walls, we tested whether the absence of NLRP3, ASC or IL-1 cytokines might modulate atherosclerosis development in LDLR-deficient mice[20], a model for familial hypercholesterolaemia. We reconstituted lethally irradiated LDLR-deficient mice with bone marrow from wild-type or NLRP3-deficient, ASC-deficient or IL-1α/β-deficient mice and subjected these mice to eight weeks of a high-cholesterol diet. In these bone marrow chimaeras, the LDLR-deficiency radioresistant parenchyma causes the animals to become hypercholesterolaemic when placed on a high-fat diet, whereas their bone marrow-derived macrophages and other leukocytes lack the NLRP3-inflammasome or IL-1 pathway components needed to respond to cholesterol crystals. No significant differences in blood cholesterol levels were observed between the different groups (wild type, $893 \pm 144\ mg\ dl^{-1}$; *ASC*$^{-/-}$, $781 \pm 114\ mg\ dl^{-1}$; *Nlrp3*$^{-/-}$,$753 \pm 132\ mg\ dl^{-1}$; *Il1a*$^{-/-}$/*b*$^{-/-}$, $832 \pm 98\ mg\ dl^{-1}$). However, mice reconstituted with NLRP3-deficient, ASC-deficient or IL-1α/b-deficient bone marrow showed significantly lower plasma levels of IL-18, an IL-1 family cytokine whose secretion is dependent on inflammasomes and a biomarker known to be elevated in atherosclerosis[21] (Fig. 4b). Additionally, mice whose bone marrow-derived cells lacked NLRP3 inflammasome components or IL-1 cytokines were markedly resistant to the development of atherosclerosis (Fig. 4c, d). The lesional area in the aortae of these mice was decreased on average by 69% in comparison with chimaeric LDLR-deficient mice that had wild-type bone marrow. These data demonstrate that activation of the NLRP3 inflammasome by bone marrow-derived cells is a major contributor to diet-induced atherosclerosis in mice. However, the contribution of NLRP3 inflammasome activation in parenchymal cells to the development of atherosclerosis cannot be assessed with this disease model and remains to be examined in mice that are doubly deficient in both LDLR and inflammasome components.

The molecules that incite inflammation in atherosclerotic lesions have presented a long-standing puzzle. Although the lesions are absolutely dependent on cholesterol, this abundant, naturally occurring molecule has been viewed as inert. Here we show that the crystalline form of cholesterol can induce inflammation. The magnitude of the inflammatory response and the mechanism of NLRP3 activation seem identical to that of crystalline uric acid, silica and asbestos[2,3,22]. All these crystals are known to provoke clinically important inflammation as seen in gout, silicosis and asbestosis, respectively.

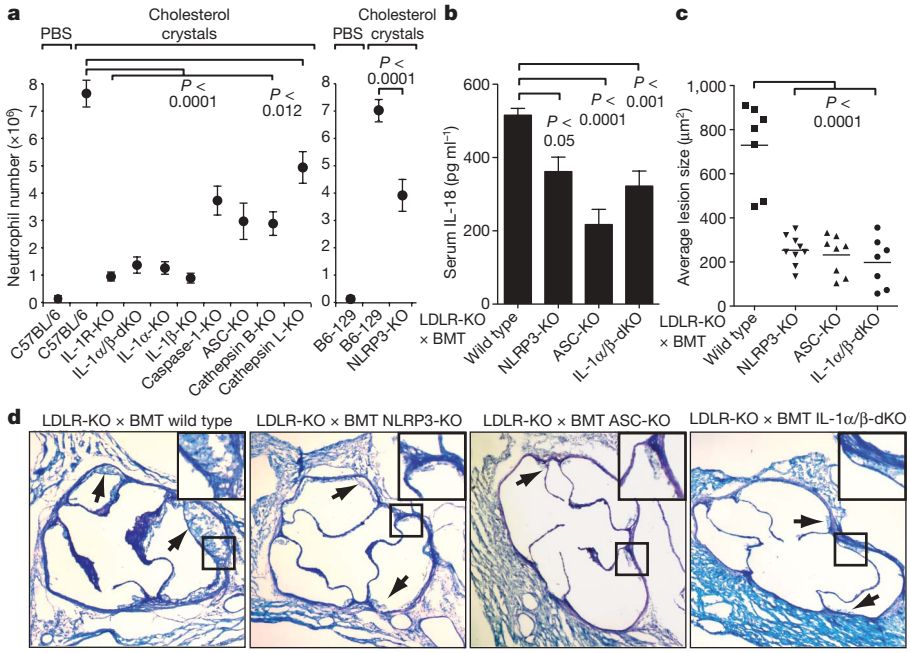

Figure 4 | The NLRP3 inflammasome mediates crystal-induced peritoneal inflammation and atherosclerosis *in vivo*. **a**, C57BL/6 ($n = 23$), B6-129 ($n = 13$) or mice deficient in genes encoding IL-1R ($n = 11$), IL-1α/β (double knockout, dKO; $n = 11$), IL-1α ($n = 4$), IL-1β ($n = 4$), caspase-1 ($n = 7$), ASC ($n = 15$), cathepsin B ($n = 10$), cathepsin L ($n = 5$) or NLRP3 ($n = 10$) were injected peritoneally with cholesterol crystals in PBS or with PBS alone (C57BL/6, $n = 14$; B6-129, $n = 4$). Peritoneal lavage cells were analysed for neutrophils after 15 h. Results are shown as means and s.e.m. for pooled groups of mice from experiments repeated two to four times. **b–d**, Female LDLR-KO mice reconstituted with C57BL/6 ($n = 7$), NLRP3-KO ($n = 9$), ASC-KO ($n = 8$) or IL-1α/β-dKO ($n = 7$) bone marrow were fed a high fat diet for 8 weeks and analysed for serum IL-18 concentration (**b**) and average aortic sinus lesion size (**c**, **d**). BMT, bone marrow transplantation. (**c**) Each dot represents the mean lesion size of serial cross-sections from individual mice. (**d**) Representative photographs of the aortic sinus stained with Giemsa. Insets show twofold magnified portions of the boxed images; arrows indicate atherosclerotic lesions.

The chronic inflammation in gout, silicosis and asbestosis is thought to derive from the inability of cells to destroy the ingested aggregates, leading to successive rounds of apoptosis and reingestion of the crystalline material[23]. In the same way, immune cells cannot degrade cholesterol; instead they depend on exporting the cholesterol to high-density lipoprotein (HDL) particles, which carry the cholesterol to the liver for disposal. The success of this or any cellular mechanism in clearing crystals may thus depend on the availability of HDL. A low concentration of HDL in the blood is one of the most prominent risk factors for atherosclerotic disease[24], and pharmacological methods of increasing HDL concentration are being actively pursued as treatments.

Even though cholesterol cannot be degraded by peripheral cells, it may be transformed to cholesteryl ester by the cellular enzyme acyl-coenzyme A:cholesterol acyltransferase (ACAT). Cholesteryl esters form droplets rather than crystals and are considered to be a storage form of cholesterol[4]. On the assumption that decreased cholesterol storage would be beneficial for decreasing atherosclerosis, ACAT inhibitors were tested in large clinical trials. Studies with two such inhibitors did not show a decrease but rather an increase in the size of the coronary atheroma[25,26]. This apparent paradox may be reconciled by our findings that the crystalline form of cholesterol, which would be expected to be increased in concentration after inhibition of ACAT, may be crucial in driving arterial inflammation. Indeed, mouse studies of ACAT deficiency show enhanced atherogenesis with abundant cholesterol crystals[27]. On the basis of our findings, therapeutic strategies that would reduce cholesterol crystals or block the inflammasome pathway would be predicted to have clinical benefit by decreasing the initiation or progression of atherosclerosis. In this context our findings also indicate novel molecular targets for the development of therapeutics to treat this disease.

METHODS SUMMARY

Cell culture media and reagents. Immortalized macrophage cell lines and bone marrow-derived cells were cultured as described[3] and primed with 10 ng ml^{-1} LPS for 2 h before the addition of inflammasome stimuli. Inhibitors were added 30 min before stimuli. Crystals and poly(dA-dT)•poly(dT-dA) were applied 6 h before supernatant was collected, and ATP (5 mM) and nigericin (10 μM) were applied 1 h before supernatant was collected. Poly(dA-dT)•poly(dT-dA) was transfected with Lipofectamine 2000 (Invitrogen). Human PBMCs were freshly isolated by Ficoll-Hypaque gradient centrifugation, grown in RPMI medium (Invitrogen), 10% FBS (Atlas Biologicals) 10 μg ml^{-1} ciprofloxacin (Celgro) at 2×10^5 cells per 96 wells, and primed with 50 pg ml^{-1} LPS for 2 h before the addition of inflammasome stimuli. Supernatants were assessed for IL-1β by enzyme-linked immunosorbent assay (ELISA) and western blotting.

Recruitment of neutrophils to peritoneal cavity. Mice were injected intraperitoneally with 2 mg of cholesterol crystals in 200 μl of PBS or with PBS alone. After 15 h, peritoneal lavage cells were stained with fluorescently conjugated monoclonal antibodies against Ly-6G (clone 1A8; Becton Dickinson) and 7/4 (Serotec) in the presence of monoclonal antibody 2.4G2 (FcgRIIB/III receptor blocker). The absolute number of neutrophils (Ly-6G-positive 7/4-positive) was determined by flow cytometry.

Bone marrow transplantation and atherosclerosis model. *Ldlr*$^{-/-}$ mice were irradiated and reconstituted with bone marrow from wild-type, *ASC*$^{-/-}$, *Nlrp3*$^{-/-}$ or *Il1a*$^{-/-}$*b*$^{-/-}$ mice. After 8 weeks of high-fat diet, the atherosclerotic regions of aortic sinuses were quantified on serially sectioned slides.

Full Methods and any associated references are available in the online version of the paper at www.nature.com/nature.

Received 25 June 2009; accepted 18 February 2010.

1. Wright, S. D. *et al.* Infectious agents are not necessary for murine atherogenesis. *J. Exp. Med.* **191,** 1437–1442 (2000).
2. Martinon, F., Petrilli, V., Mayor, A., Tardivel, A. & Tschopp, J. Gout-associated uric acid crystals activate the NALP3 inflammasome. *Nature* **440,** 237–241 (2006).
3. Hornung, V. *et al.* Silica crystals and aluminum salts activate the NALP3 inflammasome through phagosomal destabilization. *Nature Immunol.* **9,** 847–856 (2008).
4. Chang, T. Y., Chang, C. C., Ohgami, N. & Yamauchi, Y. Cholesterol sensing, trafficking, and esterification. *Annu. Rev. Cell Dev. Biol.* **22,** 129–157 (2006).
5. Small, D. M. George Lyman Duff memorial lecture. Progression and regression of atherosclerotic lesions. Insights from lipid physical biochemistry. *Arteriosclerosis* **8,** 103–129 (1988).
6. Stary, H. *et al.* A definition of advanced types of atherosclerotic lesions and a histological classification of atherosclerosis. A report from the Committee on Vascular Lesions of the Council on Arteriosclerosis, American Heart Association. *Arterioscler. Thromb. Vasc. Biol.* **15,** 1512–1531 (1995).
7. Abela, G. S. *et al.* Effect of cholesterol crystals on plaques and intima in arteries of patients with acute coronary and cerebrovascular syndromes. *Am. J. Cardiol.* **103,** 959–968 (2009).
8. Piedrahita, J. A., Zhang, S. H., Hagaman, J. R., Oliver, P. M. & Maeda, N. Generation of mice carrying a mutant apolipoprotein E gene inactivated by gene targeting in embryonic stem cells. *Proc. Natl Acad. Sci. USA* **89,** 4471–4475 (1992).
9. Zhang, S. H., Reddick, R. L., Piedrahita, J. A. & Maeda, N. Spontaneous hypercholesterolemia and arterial lesions in mice lacking apolipoprotein E. *Science* **258,** 468–471 (1992).
10. Martinon, F., Mayor, A. & Tschopp, J. The inflammasomes: guardians of the body. *Annu. Rev. Immunol.* **27,** 229–265 (2009).
11. Bauernfeind, F. G. *et al.* Cutting edge: NF-κB activating pattern recognition and cytokine receptors license NLRP3 inflammasome activation by regulating NLRP3 expression. *J. Immunol.* **183,** 787–791 (2009).
12. Hornung, V. *et al.* AIM2 recognizes cytosolic dsDNA and forms a caspase-1-activating inflammasome with ASC. *Nature* **458,** 514–518 (2009).
13. Stewart, C. R. *et al.* CD36 ligands promote sterile inflammation through assembly of a Toll-like receptor 4 and 6 heterodimer. *Nature Immunol.* **11,** 155–161 (2009).
14. Halle, A. *et al.* The NALP3 inflammasome is involved in the innate immune response to amyloid-β. *Nature Immunol.* **9,** 857–865 (2008).
15. Garin, J. *et al.* The phagosome proteome: insight into phagosome functions. *J. Cell Biol.* **152,** 165–180 (2001).
16. Yuan, X. M., Li, W., Olsson, A. G. & Brunk, U. T. The toxicity to macrophages of oxidized low-density lipoprotein is mediated through lysosomal damage. *Atherosclerosis* **133,** 153–161 (1997).
17. Chen, C. J. *et al.* Identification of a key pathway required for the sterile inflammatory response triggered by dying cells. *Nature Med.* **13,** 851–856 (2007).
18. Guarda, G. *et al.* T cells dampen innate immune responses through inhibition of NLRP1 and NLRP3 inflammasomes. *Nature* **460,** 269–273 (2009).
19. Dinarello, C. A. Immunological and inflammatory functions of the interleukin-1 family. *Annu. Rev. Immunol.* **27,** 519–550 (2009).
20. Ishibashi, S., Goldstein, J. L., Brown, M. S., Herz, J. & Burns, D. K. Massive xanthomatosis and atherosclerosis in cholesterol-fed low density lipoprotein receptor-negative mice. *J. Clin. Invest.* **93,** 1885–1893 (1994).
21. Blankenberg, S. *et al.* Interleukin-18 is a strong predictor of cardiovascular death in stable and unstable angina. *Circulation* **106,** 24–30 (2002).
22. Dostert, C. *et al.* Innate immune activation through Nalp3 inflammasome sensing of asbestos and silica. *Science* **320,** 674–677 (2008).
23. Mossman, B. T. & Churg, A. Mechanisms in the pathogenesis of asbestosis and silicosis. *Am. J. Respir. Crit. Care Med.* **157,** 1666–1680 (1998).
24. Gordon, T., Castelli, W. P., Hjortland, M. C., Kannel, W. B. & Dawber, T. R. High density lipoprotein as a protective factor against coronary heart disease. The Framingham Study. *Am. J. Med.* **62,** 707–714 (1977).
25. Nissen, S. E. *et al.* Effect of ACAT inhibition on the progression of coronary atherosclerosis. *N. Engl. J. Med.* **354,** 1253–1263 (2006).
26. Meuwese, M. C. *et al.* ACAT inhibition and progression of carotid atherosclerosis in patients with familial hypercholesterolemia: the CAPTIVATE randomized trial. *J. Am. Med. Assoc.* **301,** 1131–1139 (2009).
27. Accad, M. *et al.* Massive xanthomatosis and altered composition of atherosclerotic lesions in hyperlipidemic mice lacking acyl CoA:cholesterol acyltransferase 1. *J. Clin. Invest.* **105,** 711–719 (2000).

Supplementary Information is linked to the online version of the paper at www.nature.com/nature.

Acknowledgements This work was supported by grants from the National Institutes of Health (to E.L. and K.L.R.) and from the Deutsche Forschungsgemeinschaft (GK 1202, to M.S. and P.D.).

Author Contributions P.D., H.K., K.J.R, C.M.S., G.V., F.G.B, V.H., L.F. and E. Latz designed and performed experiments and analysed data. G.S.A. collected and prepared human samples. T.E., G.N., M.S., K.J.M., G.S.A., K.A.F. and E. Lien provided critical suggestions and discussions throughout the study. P.D., H.K., K.L.R., S.D.W., V.H. and E. Latz wrote the paper. E. Latz conceived and supervised the study.

Author Information Reprints and permissions information is available at www.nature.com/reprints. The authors declare no competing financial interests. Correspondence and requests for materials should be addressed to E.L. (eicke.latz@umassmed.edu; eicke.latz@uni-bonn.de).

METHODS

Mice. Mice were provided as follows: *Nlrp3*$^{-/-}$ and *ASC*$^{-/-}$ by Millennium Pharmaceuticals; *Casp1*$^{-/-}$ by R. Flavell; *Ctsb*$^{-/-}$ by T. Reinheckel; *Ctsl*$^{-/-}$ by H. Ploegh; and *Il1a*$^{-/-}$, *Il1b*$^{-/-}$ and *Il1a*$^{-/-}$*b*$^{-/-}$ by Y. Iwakura. B6-129 (mixed background), C57BL/*6*, *Il1r1*$^{-/-}$, *Apoe*$^{-/-}$ and *Ldlr*$^{-/-}$ mice were purchased from Jackson Laboratories. Animal experiments were approved by the University of Massachusetts and Massachusetts General Hospital Animal Care and Use Committees.

Reagents. Bafilomycin A1, cytochalasin D and zYVAD-fmk were from Calbiochem. ATP, acridine orange and poly(dA-dT)•poly(dT-dA) sodium salt were from Sigma-Aldrich, and ultra-pure LPS was purchased from InvivoGen. Nigericin, Hoechst dye, DQ ovalbumin and fluorescent choleratoxin B were purchased from Invitrogen. MSU crystals were prepared as described[17].

Cholesterol crystal preparation. Tissue-culture grade or synthetic cholesterol was purchased from Sigma, solubilized in hot acetone and crystallized by cooling. After six cycles of recrystallization, the final crystallization was performed in the presence of 10% endotoxin-free water to obtain hydrated cholesterol crystals. Cholesterol crystals were analysed for purity by electron impact gas chromatography–mass spectrometry and thin-layer chromatography with the use of silica gel and hexane-ethyl acetate (80:20) solvent. Crystal size was varied with a microtube tissue grinder. Fluorescent cholesterol was prepared by the addition of DiD or DiI dye (Invitrogen) in PBS.

ELISA and western blotting. ELISA measurements of IL-1β (Becton Dickinson) and IL-18 (MBL International) were made in accordance with the respective manufacturer's directions. Experiments for caspase-1 western blot analysis were performed in serum-free DMEM medium. After stimulations, cells were lysed by the addition of a 10× lysis buffer (10% Nonidet P40 in Tris-buffered saline (10 mM Tris-HCl, pH 7.5, 150 mM NaCl) and protease inhibitors), and post-nuclear lysates were separated by 4–20% reducing SDS–PAGE. Anti-mouse caspase-1 polyclonal antibody was provided by P. Vandenabeele. Anti-human cleaved IL-1β (Cell Signaling) from human PBMCs was analysed in serum-free supernatants as above without cell lysis.

Confocal microscopy. *Apoe*$^{-/-}$ mice maintained in a pathogen-free facility were fed with a Western-type diet (Teklad Adjusted Calories 88137; 21% (w/w) fat, 0.15% (w/w) cholesterol, 19.5% (w/w) casein; no sodium cholate) starting at 8 weeks of age; this continued for 2, 4, 8 or 12 weeks (three mice in each group). Mice were killed and hearts were collected as described[28]. Hearts were sectioned serially at the origins of the aortic valve leaflets, and every third section (5 μm thick) was stained with haematoxylin/eosin and imaged by light microscopy. Adjacent sections were fixed in 4% paraformaldehyde, blocked and permeabilized (10% goat serum and 0.5% saponin in PBS) and stained for 1 h at 37 °C with fluorescent primary antibodies against macrophages (MoMa-2; Serotec), dendritic cells (CD11c; Becton Dickinson) or neutrophils (anti-Neutrophil; Serotec) for imaging by confocal microscopy.

Human atherosclerotic lesions were obtained directly after autopsy, serially sectioned at 2–3-mm intervals, and frozen sections (5 mm thick) were prepared as above. Parallel sections were stained with Masson's trichrome stain. Tissues were prepared for microscopy as above. Macrophages were stained with anti-CD68 (Serotec); smooth muscle cells were revealed with fluorescent phalloidin (Invitrogen). Human and mouse samples were counterstained with Hoechst dye to reveal nuclei. The atherosclerotic lesions were imaged on a Leica SP2 AOBS confocal microscope where immunofluoroscence staining was revealed by standard confocal techniques, and crystals were observed with laser reflection using enhanced transmittance of the acousto-optical beam splitter as described[3]. Laser reflection and fluorescence emission occurs at the same confocal plane in this setup. The mean lesion area, amount of crystal deposition and monocyte marker presence were quantified from three digitally captured sections per mouse (Adobe Photoshop CS4 Extended). For quantification of the crystal mass and macrophages present, the sum of positive pixels (laser reflection and fluorescence, respectively) was determined and the area was calculated from the pixel size.

Confocal microscopy of mouse macrophages was performed as described[3]. DQ ovalbumin fluoresces only on proteolytic processing, marking phagolysosomal compartments in macrophages.

Acridine orange lysosomal damage assay. This assay was performed by flow cytometry as described[3].

Bone marrow transplantation and atherosclerosis model. Eight-week-old female *Ldlr*$^{-/-}$ mice were lethally irradiated (11 Gy). Bone marrow was prepared from femurs and tibiae of C57BL/6, *Nlrp3*$^{-/-}$, *ASC*$^{-/-}$ and *Il1a*$^{-/-}$*Il1b*$^{-/-}$ donor mice, and T cells were depleted with complement (Pel-Freez Biologicals) and anti-Thy1 monoclonal antibody (M5/49.4.1; American Type Culture Collection). Irradiated recipient mice were reconstituted with 3.5×10^6 bone marrow cells administered into the tail vein. After four weeks, mice were fed with a Western-type diet (Teklad Adjusted Calories 88137; 21% (w/w) fat, 0.15% (w/w) cholesterol, 19.5% (w/w) casein; no sodium cholate) for eight weeks. Mice were killed and perfused intracardially with formalin. Hearts were embedded in OTC (Optimal Cutting Temperature) (Richard-Allan Scientific) medium, frozen, and serially sectioned through the aorta from the origins of the aortic valve leaflets; every single section (10 μm thick) throughout the aortic sinus (800 μm) was collected. Quantification of average lesion area was performed from 12 sections stained with haematoxylin/eosin or Giemsa from each mouse by two independent investigators, with virtually identical results. Serum cholesterol levels were determined by enzymatic assay (Wako Diagnostics), and serum IL-18 was measured by SearchLight protein array technology (Aushon Biosystems).

Statistical analyses. The significance of differences between groups was evaluated by one-way analysis of variance (ANOVA) with Dunnett's post-comparison test for multiple groups to control group, or by Student's *t*-test for two groups. R^2 was calculated from the Pearson correlation coefficient. Analyses were performed with Prism (GraphPad Software, Inc.).

28. Moore, K. J. *et al.* Loss of receptor-mediated lipid uptake via scavenger receptor A or CD36 pathways does not ameliorate atherosclerosis in hyperlipidemic mice. *J. Clin. Invest.* **115**, 2192–2201 (2005).